Int. J. Electrochem. Sci., 16 **(2021)** Article ID: 210739, doi: 10.20964/2021.07.69

International Journal of
ELECTROCHEMICAL
SCIENCE
www.electrochemsci.org

Short Communication

Synthesis and Electrochemical Behavior of Na^+ and Zr^{4+} Doped $LiMnPO_4$/C as Potential Cathode Material for Li-ion Batteries

ChenChen Han[1], Xiang Yao[1,2,], Hualing Tian[1,2], Yanjun Cai[1], Zhi Su[1,2,*]*

[1] College of Chemistry and Chemical Engineering, Xinjiang Normal University
[2] Xinjiang Key laboratory of energy storage and photoelectrocatalytic materials
[*]E-mail: yaoxiangxjnu@163.com, suzhixj@sina.com

Received: 4 April 2021 / *Accepted:* 12 May 2021 / *Published:* 31 May 2021

By using a simple sol–gel method, several compounds, including $LiMnPO_4$/C, $Li_{0.9}Na_{0.1}MnPO_4$/C, and $Li_{0.9}Na_{0.1}Mn_{0.98}Zr_{0.02}PO_4$/C, were successfully synthesised. We studied the effects of partial substitution of Li^+ and Mn^{2+} with Na^+ and Zr^{4+} doped in $LiMnPO_4$/C and the electrochemical energy storage behavior of the final product. At 0.05 C, discharge specific capacity of $Li_{0.9}Na_{0.1}Mn_{0.98}Zr_{0.02}PO_4$/C can be 159.4 mAh/g, which was much better than unmodified $LiMnPO_4$/C (121.9 mAh/g). Capacity retention rate was 98% after 50 cycles. Appropriate concentrations of Na^+ and Zr^{4+} doping at different cation positions can effectively improve $LiMnPO_4$/C electrochemical behavior.

Keywords: Li-ion battery; $LiMnPO_4$; cation doping; Electrochemical behavior

1. INTRODUCTION

With the rapid growth of human population and the widespread use of the electric vehicles and hybrid vehicles, rechargeable batteries have increasingly become an indispensable element with direct applications to provide electrical energy. Li-ion batteries is the hot spot recently because of its high output voltage, high capacity, as well as stable embedded material structures[1,2]. Cathode materials, which have been the focus of scientists' studies, are considered the core of lithium-ion batteries. The materials have decisive effects on capacity and electrochemical behavior of Li-ion batteries.

Currently, various polyanions, $LiMPO_4$ (M = Fe, Mn, Ni, Co) with a typical crystal morphology, have received considerable attention as cathode materials[3,4] since they are environmental compatible and cost effective. Another reason that makes them popular is their high capacity. The most representative compound among these materials is $LiFePO_4$, which is commercialised in various industries. However, low energy density and discharge voltage limit its

development[5]. Another olivine material, $LiMnPO_4$, with a capacity of 170 mAh/g, is gradually developed. $LiMnPO_4$ provides a higher charge–discharge voltage and theoretical energy density of 4.1 V (vs Li/Li^+) and 701 Wh/kg, respectively, than $LiFePO_4$. Moreover, the abundant reserves of manganese in nature make it a promising material. $LiMnPO_4$ presents some inherent limitations. For instance, a phase mismatch exists at the boundary between $LiMnPO_4$ and $MnPO_4$, and through the Jahn–Teller effect of Mn^{3+}, the crystal structure rapidly collapses with a decreased cycle performance[7,8]. In addition, the low conductivity and diffusion coefficients of $LiMnPO_4$ can be attributed to the large energy gap and high diffusion activation barrier[9,10]. To overcome these shortcomings, researchers have conducted numerous studies on $LiMnPO_4$. Most studies have focused on the following aspects: controlling the particle size, tailoring the particle morphology[11-13], coating conductive materials on surfaces[14,15], and doping metal cations at appropriate sites[16-23]. Currently, for the $LiMnPO_4$ lattice, the most common method is the doping of Mn sites with Fe^{2+}[16-19], Mg^{2+}[16,17,19,20-21], Zn^{2+}[22,23], and Zr^{4+}[20,21]. Hu et al. produced $LiMn_{0.9}Fe_{0.05}Mg_{0.05}PO_4$, a compound with 121 mAh/g discharge capacity, which is considerably larger than pure $LiMnPO_4$ (67 mAh/g) at 0.2 C [24]. It was reported that co-doping effect of Fe^{2+} and Zn^{2+} in $LiMn_{0.9}Fe_{0.1-x}Zn_xPO_4/C$. Due to its electrochemical inactivity, Zn^{2+} hinders the Jahn–Teller effect of Mn^{3+}, thereby improving battery reversibility[22]. Furthermore, studies have shown that Zr^{4+} plays a positive role in the structural stability of crystals. This property of Zr^{4+} may be caused by its large ionic radius. This radius leads to an increase in the separation between crystal layers and enables the free extraction/insertion of lithium ions[25]. Because high valence of Zr^{4+}, relative content of Mn^{3+} in an electrolyte decreases, thereby causing a decrease in Jahn–Teller deformation and the further improvement of structure stability[26]. Lee et al. reported a replacement strategy by the incorporation of Mg^{2+} and Zr^{4+}. The reversible capacity increases and polarisation decreases after the usage of this strategy, which may be caused by the incorporation of Mg^{2+} and/or Zr^{4+} within a certain lattice tolerance range. Then a decrease in crystal structure distortion forms with increased diffusion kinetics[20]. Their results also indicated that irreversible capacity loss in the first charge–discharge cycle of $LiMn_{0.88}Mg_{0.1}Zr_{0.02}PO_4$ was lower than that of $LiMnPO_4$. Therefore, the enhancement of electrochemical performance is feasible via doping high valence Zr^{4+} in $LiMnPO_4/C$ (LMP) crystal lattices.

Recently, studies have gradually investigated doping in Li sites. Sodium is one of the most abundant elements on the earth. Because Na and Li are near to each other in the periodic table, they are similar in electronic structures and chemical properties. Because the Na^+ radius is larger Li^+ radius, Na^+ increased the lithium-ion diffusion range during intercalation and deintercalation[27]. Hence, the partial substitution can potentially improve performance. Rajammal et al. first showed that substitutional Na^+ doping in $LiMnPO_4$ leads to a decrease in irreversible capacity loss. Compared with undoped $LiMnPO_4$ (86.26 mAh/g), the maximum discharge capacity of $Li_{0.97}Na_{0.03}MnPO_4$ is higher (92.45 mAh/g). And its capacity retention rate can be 84.15% even after 60 cycles[28]. Khalfaouy et al. used the solution combustion method to synthesise the cathode material of $Li_{0.97}Na_{0.03}MnPO_4/C$ with discharge of 136.7 mAh/g and found that an appropriate amount of Na^+ in $LiMnPO_4$ reduces the charge transfer resistance by improving lithium ion movement within the intercalation layer[29]. Zhang et al. synthesised $Li_{0.9}Na_{0.1}MnPO_4/C$ with 152 and 122.3 mAh/g at 0.05 and 10 C, respectively[27], which is quite marvellous. In addition, Li et al. used solvothermal methods to

fabricate $Li_{0.97}Na_{0.03}Mn_{0.8}Fe_{0.2}PO_4/C$ nanocapsules and revealed doping with Na^+ and Fe^{2+} to be effective for high structure and chemical stability[30].

With the aforementioned advantages, we used a simple sol–gel method to substitute some Li and Mn sites in the $LiMnPO_4$ cathode material with Na^+ and Zr^{4+}. The structure, morphology, and properties were characterised. Compared with pure-phase undoped $LiMnPO_4$, the $Li_{0.9}Na_{0.1}Mn_{0.98}Zr_{0.02}PO_4$ material exhibited considerably improved electrochemical performance. In the energy storage applications of $LiMnPO_4$-based materials, the doping of Li sites remains in the development stage. However, few studies have investigated co-doping at Li and Mn sites. The results of this study provided novel inspiration for $LiMnPO_4$ modifications.

2. EXPERIMENTAL DESIGN

2.1. Material preparation

The reagents used in this experiment are analytically pure. $Mn(CH_3COO)_2{\cdot}4H_2O$, $CH_3COOLi{\cdot}2H_2O$, and CH_3COONa were dissolved in 50 mL of DMF at a certain stoichiometric ratio. Subsequently, an accurate amount of H_3PO_4 was weighed in a beaker, and then a solution was obtained with a certain proportion of glucose, used as the carbon source, and 30 mL DMF solution. A magnetic stirrer was used to make the solution well-distributed and a certain molar ratio of $C_{16}H_{36}O_4Zr$ was added dropwise to the mixed solution. Finally, the sol–gel mixture was obtained after stirring the solution at 80 °C. The mixture was dried (12 h, 80 °C) and calcined (2 h, 350 °C) in argon atmosphere. Then it was calcined for another 16 h at 700 °C. Calcined sample was evenly ground, and the $Li_{1-y}Na_yMn_{1-x}Zr_xPO_4/C$ composite material was achieved.

2.2. Characterization

The X-ray diffraction (Bruker D2), with Cu Kα1 radiation of 0.15418 nm at 40 kV and 200 mA and 2θ range of 10°–70°, was used to detect and record the crystal structure of synthesised powder sample. Transmission electron microscopy (TEM, FEI Tecnai 20) was used to determine the surface morphology and lattice spacing of the crystallised material.

2.3 Electrochemical measurements

To obtain a uniformly mixed slurry, 75 wt% of active material ($Li_{0.9}Na_{0.1}Mn_{0.98}Zr_{0.02}PO_4/C$), 20 wt% of super P as the conductive agent, and 5 wt% of PVDF as the binder were added to a milling tank with NMP included. This mixture was ground for 6 h and the obtained product was evenly placed on a piece of Al foil before vacuum drying at 110 °C for 12h. The active material was cut to a size of 12 × 12 mm from the aluminium foil with an active material loading 2 to 3 mg cm^{-2}. In the electrochemical test, a lithium disc was applied as anode. Electrolyte was composed of 1 M $LiPF_6$, which was dissolved in the mix solvents of EC, EMC and DMC. The volume ratio of the three solvents

was 1:1:1. Celgard 2400 was used as the membrane. The button-type battery with its serial number CR2025 was assembled in a glove box.

The battery was tested by a test system (LAND, CT-2001A). Voltage was increased from 2.5 to 4.5 V. Battery was then charged at 4.5 V for 4 h. Subsequently, the rate corresponding to the charging process was used to discharge the battery to 2.5 V. Cyclic voltammetry was tested in an electrochemical workstation (CHI660e) at voltage of 2.5–4.5 V at 0.1 $mV \cdot s^{-1}$ under ambient conditions. Frequency was 10 kHz to 10 mHz with 5 mV applied AC modulation. The electrochemical impedance (EIS) between the two electrodes was measured.

3. RESULTS AND DISCUSSION

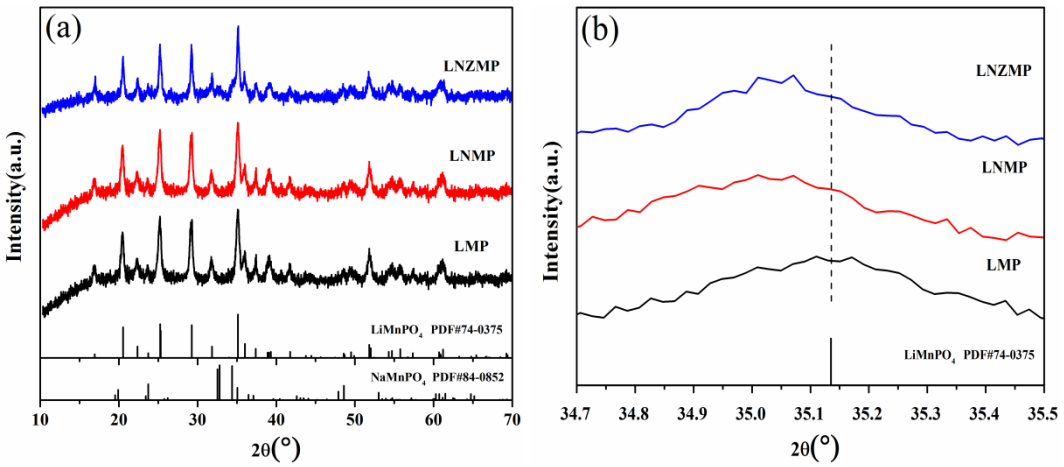

Figure 1. (a) XRD patterns of LMP, $Li_{0.9}Na_{0.1}MnPO_4/C$ (LNMP), and $Li_{0.9}Na_{0.1}Mn_{0.98}Zr_{0.02}PO_4/C$ (LNMZP). (b) XRD partial zoom results of LMP, LNMP, and LNMZP for 2θ of 34.7°–35.5°.

To see the influences of Na^+ and Zr^{4+} doping, $LiMnPO_4$ (LMP), $Li_{0.9}Na_{0.1}MnPO_4$ (LNMP), and $Li_{0.9}Na_{0.1}Mn_{0.98}Zr_{0.02}PO_4$ (LNMZP) cathode materials were successfully prepared. The crystal structure was analysed through XRD (Fig. 1a). Main diffraction peaks were attributed to the orthorhombic $LiMnPO_4$ olivine structure (PDF#74-0375). Residual carbon obtained after high-temperature calcination was amorphous. Hence, no carbon diffraction peak was observed. In addition, no obvious diffraction peak associated with Na or Zr appeared in the doped samples, indicating that the dopants were wonderfully placed into the crystal. Figure 1b presents a partially enlarged view of the diffraction pattern with the 2θ of 34.7°–35.5°. The lattice spacing after Na^+ doping is larger than before, since the atomic radius of Na^+ is bigger than Li^+. Therefore, the main diffraction peak shifts slightly towards a small angle (Fig.1b).

The TEM image reveals the morphology, particle size, and internal structure of the crystal (Fig. 2). Figures 2a, c, and e illustrates the morphologies of LMP, LNMP, and LNMZP samples, respectively, under low magnification. All the three materials show the nanoparticular morphology with an average particle size of 50–70 nm. Figure 2b, d, and f shows that a thin carbon layer, which provided excellent electrochemical performance, was formed on the particle surfaces under high

magnification. Lattice fringes in the high-resolution TEM images are assigned to the (111), (011), and (111) crystal planes of $LiMnPO_4$ (PDF#74-0375). Some particles in Na^+-doped LNMP and LNMZP show (211) and (220) crystal planes from $NaMnPO_4$ (PDF#84-0852), which match the XRD patterns quite well.

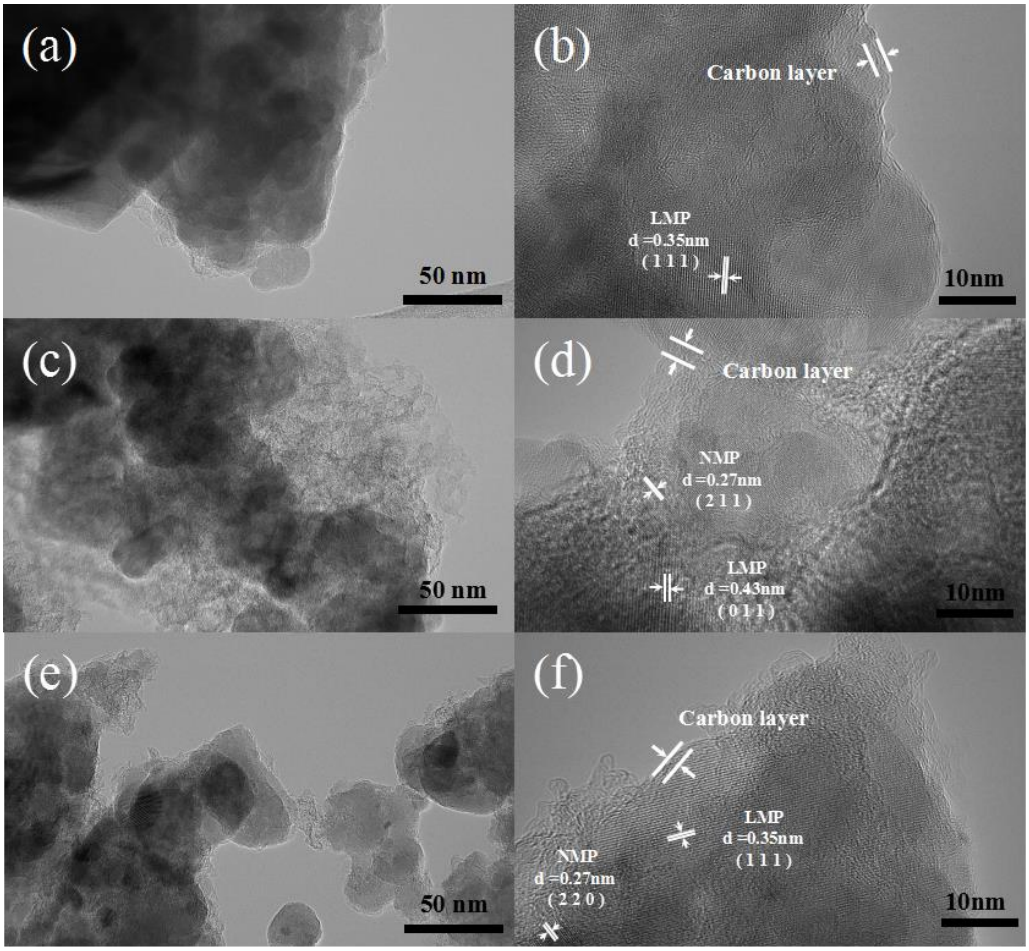

Figure 2. TEM patterns of (a) LMP, (c) LNMP, and (e) LNMZP. High-resolution TEM of (b) LMP, (d) LNMP, and (f) LNMZP.

The charge–discharge tests obtained at room temperature for undoped $LiMnPO_4$/C and the doped samples at the 0.05 C rate. All samples showed high discharge voltage plateaus at approximately 4 V, which is in a strong agreement with the Mn^{3+}/Mn^{2+} redox potential in $LiMnPO_4$. No other discharge plateau was observed, indicating that the incorporation of Na^+ and Zr^{4+} did not change the original electrochemical reaction. Discharge specific capacity was only 121.2 mAh/g in the first LMP cycle, which improved to 139.8 mAh/g with Na^+ doping. After doping with both Na^+ and Zr^{4+}, the discharge specific capacity reached the highest (159.4 mAh/g). As shown in Table 1, the reversible capacity of $LiMn_{0.98}Zr_{0.02}PO_4$ reported in the literature was increased by 18.8mAh/g compared to $LiMnPO_4$[20]. In addition, it can be found in the table that the reversible capacity of materials doped with Na^+ are all higher than that of $LiMnPO_4$[27-32].These phenomena is consistent with the higher discharge specific capacity of the LNMZP we synthesized, indicating that a certain

amount of Na^+ and Zr^{4+} are doped in Li site and Mn, respectively. Therefore Na^+ and Zr^{4+} have the effect of jointly increasing the reversible capacity.

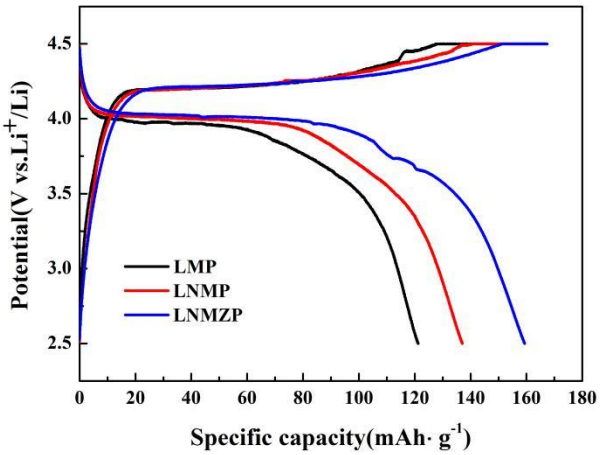

Figure 3. First charge/discharge patterns of LMP,LNMP and LNMZP at 0.05C.

Table 1. Comparison of electrochemical performance of different phosphate-based cathode materials

Materials	Current density	Initial discharge capacity[mAh/g]	Cycle number	Capacity Retention	ref
$LiMnPO_4$	7.5 mA/g	91.2	30	68%	[20]
$LiMn_{0.98}Zr_{0.02}PO_4$		110	30	87%	
$LiMnPO_4$	0.2 C	86.3	25	83.3%	[27]
$Li_{0.97}Na_{0.03}MnPO_4$		92.5	25	87.6%	
$LiMnPO_4$	0.05 C	126.9	50	81.6%	[28]
$Li_{0.97}Na_{0.03}MnPO_4$		136.7	50	90.2%	
$LiMnPO_4$	0.05 C	110.5	200	94.8%	[29]
$Li_{0.97}Na_{0.03}Mn_{0.8}Fe_{0.2}PO_4/C$		141.7	200	96.7%	
$LiMnPO_4$	0.05 C	125	200	65%	[30]
$Li_{0.9}Na_{0.1}MnPO_4$		152	200	93.8%	
$LiMnPO_4$	0.05 C	121.2	50	90.8%	This work
$Li_{0.9}Na_{0.1}MnPO_4$		139.8	50	95%	
$Li_{0.9}Na_{0.1}Mn_{0.98}Zr_{0.02}PO_4$		159.4	50	98%	

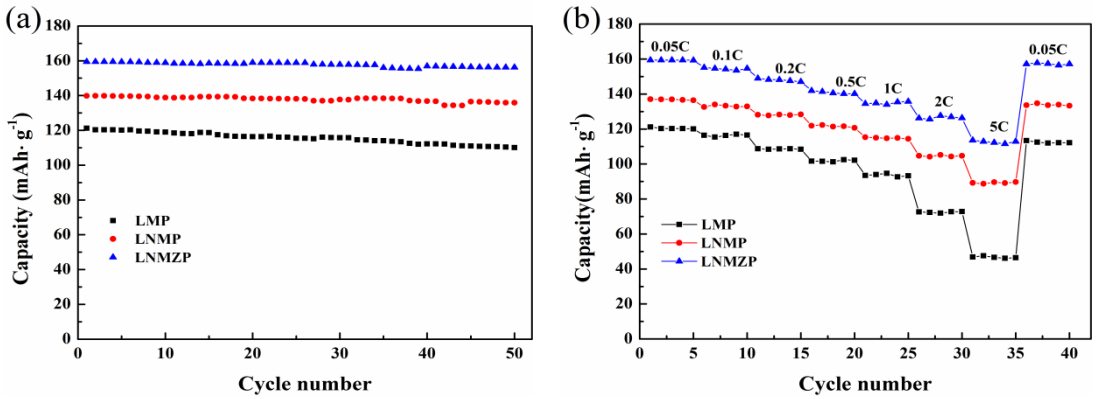

Figure 4. Cycling performance of LMP, LNMP, and LNMZP: (a) Discharge capacity and (b) different rate performance.

Figure 4a illustrates the performance of the undoped and doped $LiMnPO_4$/C samples for 50 cycles under the 0.05 C rate condition. After 50 charge–discharge cycles, LMP, LNMP, and LNMZP exhibited the remaining capacities of 110.1, 130.2 and 156.2 mAh/g, respectively, with the corresponding retention rates of 90.8%, 95% and 98%, respectively. $LiMnPO_4$/C capacity decay during cycling mainly resulted from the Jahn–Teller distortion. The larger was the distance between Mn^{2+}, the smaller was the influence of the John–Teller effect on $LiMnPO_4$/C. Na^+ substitution led to an increase in the Mn–Mn distance, thereby decreasing the Jahn–Teller effect. By contrast, Zr^{4+} addition led to a decrease in the relative concentration of Mn^{3+}, thereby effectively suppressing the Jahn–Teller effect. These two aspects together improved the structural stability of materials. From the comparison of the cycle stability of different materials in Table 1, it is not difficult to see that the stability of $LiMn_{0.98}Zr_{0.02}PO_4$ has been improved by about 20%, which may be related to the formation of a film on the surface of the material[20]. In addition, according to other documents on the original sample doped with Zr^{4+}, a conclusion can be drawn that all samples doped with a small amount of zirconium can show good cycle performance[35-39]. The partial substitution of Na^+ for Li^+ increases the distance between Mn-Mn, which weakens the John-teller effect of the crystal structure and produces stronger stability[27-30].Based on the above conditions, the LNMZP material we synthesised was the highest capacity retention rate of 98%, with almost no capacity decay.

Figure 4b shows the discharge capacities of the doped and undoped $LiMnPO_4$/C at 0.05–5 C discharge rate. When discharge rate increased gradually, the capacity of the three materials decreased to different degrees; LNMZP showed the highest capacities of 159.4, 155.1, 149, 141.9, 134.5, 126.2, and 113.6 mAh/g at the discharge rates of 0.05, 0.1, 0.2, 0.5, 0.5, 2, and 5 C. After returning to 0.05 C, the capacity recovered to 156.3 mAh/g.Xu et al. and Li et al. also found better rate performance in Zr^{4+} doped $Li_3V_{1.87}Zr_{0.1}(PO_4)_3$ and $Li_{1.035}Zr_{0.02}FePO_4$/C at 5C and 20C, respectively[33,34]. $Li_{0.9}Na_{0.1}MnPO_4$/C synthesized by Zhang et al. can still maintain a capacity of 122.3 at 10C[30], which shows consistent high-rate discharge performance with the LNMZP synthesized by me.Therefore, Na^+ and Zr^{4+} doping can considerably improve $LiMnPO_4$ rate performance.

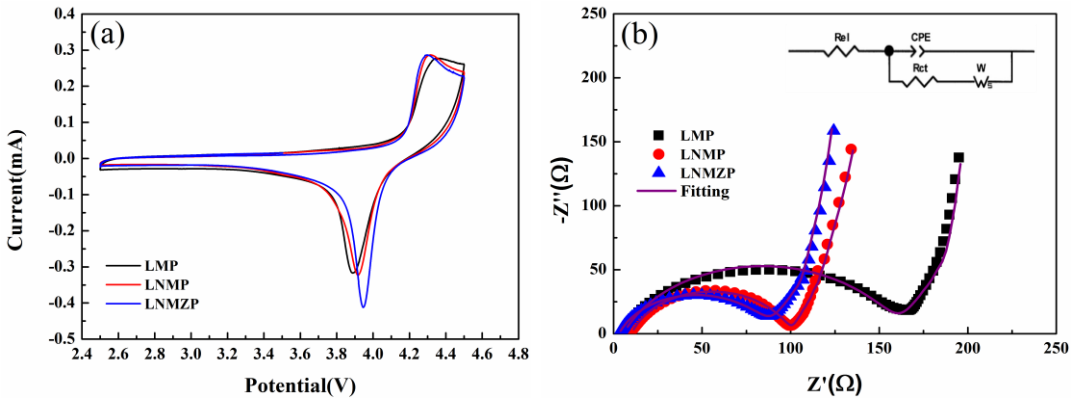

Figure 5. (a) CV curves of LMP, LNMP, and LNMZP at 0.1 $mV \cdot s^{-1}$. (b) Electrochemical impedance curves of LMP, LNMP, and LNMZP.

Table 2. Electrochemical parameters for the EIS results

Materials	$R_{ct}(\Omega)$	Ws(Ω)	CPE
$LiMnPO_4$	155.8	320.5	$1.04*10^{-5}$
$Li_{0.9}Na_{0.1}MnPO_4$	90.28	230.2	$2.03*10^{-5}$
$Li_{0.9}Na_{0.1}Mn_{0.98}Zr_{0.02}PO_4$	85.77	177.1	$2.09*10^{-5}$

Figure 5a presents the comparison of the CV curves between 2.5 and 4.5 V (vs. Li/Li^+) for LMP, LNMP and LMMZP. The scan rate was set to 0.1 mV/s. Two redox peaks, which are consistent with Mn^{2+}/Mn^{3+} reaction, can be seen in the plots. The smaller is the potential difference between the redox pairs, the easier is the redox process. The redox potential difference of synthesised LNMZP was close to 0.34 V, which is the lowest among all the samples. Low utilization and high polarization of $LiMnPO_4$ to sluggish kinetics of lithium transport within the particles ,The incorporation of Zr^{4+} can effectively improve the transmission efficiency of lithium ions[20]. Secondly, in the sample doped with Na^+, the current peak intensity is enhanced, which also shows that the electrochemical performance is improved[27,28,31].This result is consistent with the situation of the LNMZP we synthesized. Hence, Na^+ and Zr^{4+} doping improves redox reaction reversibility and reaction kinetics, which leads to a decrease in the polarization degree.

Figure 5b presents the electrochemical impedance spectra of absolute $LiMnPO_4$/C and doped $LiMnPO_4$/C. All spectra are composed of a semicircular curve together with a tilted straight line, which represent high-frequency and low-frequency regions, respectively. According to the inserted equivalent circuit, we drew the purple fitting curve, the combined curve and the fitting values obtained in Table 2. We found that the Rct of the samples LMP, LNMP, and LNMZP are 155.8, 90.28, 85.77Ω, respectively. The results obtained show that LNMZP has the smallest Rct. This result may be related to the increase in the ion conductivity, which leads to improved charge–discharge capacity. Therefore, materials doped with Na^+ and Zr^{4+} have a decreased charge transfer resistance with an effectively

increased electron conductivity. This finding is consistent with good charge–discharge and cycle performance.

4. CONCLUSIONS

By substituting Li^+ and Mn^{2+} with Na^+ and Zr^{4+}, respectively, the $Li_{0.9}Na_{0.1}Mn_{0.98}Zr_{0.02}PO_4$ cathode material was effectively prepared by sol–gel process. The high crystal structure quality was proved by XRD. The electrochemical results showed that Na^+ (0.1) and Zr^{4+} (0.02) doping can improve the cycle performance, rate performance, and diffusion properties of $LiMnPO_4$ cathodes. $Li_{0.9}Na0.1Mn_{0.98}Zr_{0.02}PO_4$ offers a substantially improved stability of the olivine with the inhibited dissolution of Mn^{3+} in the electrolyte. The effective replacement Li with Na elements in lithium-ion batteries also provides advantages for the sustainable development of resources.

ACKNOWLEDGEMENT
The study is funded by the National Natural Science Foundation of Xinjiang (2018D01B30).

References

1. J.W. Choi, D. Aurbach, *Nat. Rev. Mater.,* 1 (2016) 1.
2. S. Chu, Y. Cui, N. Liu, *Nat. Mater.,* 16 (2017) 16.
3. H. Yang, Y. Wang, J.G. Duh, *ACS. Sustain. Chem. Eng.,* 6 (2018) 13302.
4. X. Yan, D. Sun, Y. Wang, Z. Zhang, W. Yan, J. Jiang, F. Ma, J. Liu, Y. Jin, K. Kanamura, *ACS. Sustain. Chem. Eng.,* 5 (2017) 4637.
5. C. Zhu, Z. Wu, J. Xie, Z. Chen, J. Tu, G. Cao, X. Zhao, *J. Mater. Sci. Technol.,* 34 (2018) 1544.
6. J. Ni, Y. Kawabe, M. Morishita, M. Watada, T. Sakai, *J. Power Sources,* 196 (2011) 8104.
7. Y. Wang, H. Yang, C.Y. Wu, J.G. Duh, *J. Mater. Chem.,* A5 (2017) 18674.
8. L. Bao, Y. Chen, G. Xu, T. Yang, Z. Ji, Eur. *J. Inorg. Chem.,* 2018 (2018) 1533.
9. L. Esmezjan, D. Mikhailova, M. Etter, J. Cabana, C.P. Grey, S. Indris, H. Ehrenberg, *J. Electrochem. Soc.,* 166 (2019) A1257.
10. I. Bezza, M. Kaus, R. Heinzmann, *J. Phys. Chem. C.,* 119 (2015) 9016.
11. V. Ragupathi, P. Panigrahi, G.S. Nagarajan, *Appl. Surf. Sci.,* 495 (2019) 143541.
12. X. Pan, Z. Gao, L. Liu, F. Xiao, F. Xiao, S. Xie, R. Yi, *J. Alloy. Compd.,* 783 (2019) 468.
13. N.H. Kwon, H. Yin, T. Vavrova, J.H-W. Lim, U. Steiner, B. Grobety, K.M. Fromm, *J. Power Sources,* 342 (2017) 231.
14. H.C. Dinh, S. Mho, Y. Kang, I.H. Yeo. *J. Power. Sources,* 244 (2013) 189.
15. Z.Z. Xie, K. Chang, B. Li, H.W. Tang, X.N. Fu, Z.R. Chang, X.Z. Yuan, H.J. Wang, *Electrochim. Acta,* 189 (2016) 205.
16. M. Köntje, M. Memm, P. Axmann, M. Wohlfahrt-Mehrens, *Prog. Solid State Chem.,* 42 (2014) 106.
17. J. Nava-Avendaño, M.R. Palacín, J. Oró-Solé, A. Ponrouch, J.M. Tarascon, N. Recham, *Solid State Ionics,* 263 (2014) 157.
18. K. Du, L.H. Zhang, Y.B. Cao, Z.D. Peng, G.R. Hu, *Mater. Chem. Phys.,* 136 (2012) 925.
19. G. Yang, H. Ni, H. Liu, P. Gao, H. Ji, S. Roy, J. Pinto, X. Jiang, *J. Power Sources,* 196 (2011) 4747.

20. J.W. Lee, M.S. Park, B. Anass, J.H. Park, M.S. Paik, S.G. Doo, *Electrochim. Acta,* 55 (2010) 4162.
21. T. Shiratsuchi, S. Okada, T. Doi, J.I. Yamaki, *Electrochim. Acta,* 54 (2009) 3145.
22. H. Yi, C. Hu, X. He, H. Xu, *Ionics.,* 21(2015) 667.
23. H. Fang, H. Yi, C. Hu, B. Yang, Y. Yao, W. Ma, Y. Dai*, Electrochim. Acta.,* 71 (2012) 266.
24. C. Hu, H. Yi, H. Fang, B. Yang, Y. Yao, W. Ma, Y. Dai, *Electrochem. Commun.,* 12 (2010) 1784.
25. L. Li, E. Han, L. Zhu, S. Qiao, C. Du, H. Liu, *Solid State Ionic.,* 346 (2020) 115220.
26. W. Kong, H. Wang, Y. Zhai, L. Sun, X. Liu, *J. Phys. Chem. C.,* 122 (2018) 25909.
27. J. Zhang, S.H. Luo, Q.X. Ren, D.J. Zhang, Y. Qin, *Appl Surf Sci.,* 530 (2020) 146628.
28. K. Rajammal, D. Sivakumar, N. Duraisamy, K. Ramesh, S. Ramwsh, *B. Mater. Sci.,* 40 (2017) 171.
29. R.E. Khalfaouy, A. Addaou, A. Laajeb, A. Lahsini, *J. Alloy Compd.,* 775 (2019) 836.
30. R. Li, C. Fan, W. Zhang, M. Tan, T. Zeng, S. Han, *Ceram. Int.,* 45 (2019) 10501.
31. J. Li, S. Luo, Y. Sun, J. Li, J. Zhang, T.F. Yi, *Ceram. Int.,* 45 (2019) 4849.
32. J. Zhang, S.H. Luo, L.L. Sui, Y.Y. Sun, Y.H. Niu, *J. Alloy Compd.,* 768 (2018) 991.
33. J. Xu, G. Chen, H. Zhang, W. Zheng, Li, Y, *J Appl Electrochem.,* 45 (2015) 123.
34. Y. Li, Y. Zhang, J. Ma, L.Yang, X. Li, E. Zhao, C. Yang, *J Electrochem Soc.,* 166 (2019) A410.
35. C.S. Yoon, M.J. Choi, D.W. Jun, Q.Zhang, P. Kaghazchi, K.H. Kim, Y.K Sun, *Chem Mater.,* 30 (2018) 1808.
36. F. Schipper, H. Bouzaglo, M. Dixit, E.M. Erickson, T. Weigel, M.D. Talianker, *Adv Energy Mater.,* 8 (2018) 1701682.
37. D.Wang, X. Li, Z. Wang, H. Guo, Y. Xu, Y. Fan, J. Ru, *Electrochim Acta.,* 188 (2016) 48.
38. L.Hou, X. Qin, X.Gao, T. Guo, X. Li, J.Li, *J. Alloy Compd.,* 774 (2019) 38.
39. L. Li, E. Han, L. Zhu, S. Qiao, C. Du, H. Liu, *Solid State Ionics.,* 346 (2020) 115220.